Joint Channel and Impulsive Noise Estimation in Underwater Acoustic OFDM Systems

Peng Chen, Yue Rong, Sven Nordholm, and Zhiqiang He

***Abstract*—Impulsive noise is one key factor that limits the performance of underwater acoustic (UA) communications. In this paper, two pilot-subcarrier based algorithms are proposed to improve the performance of channel estimation and impulsive noise mitigation for UA orthogonal frequency-division multiplexing (OFDM) systems. The first algorithm jointly estimates the channel and the impulsive noise based on the least-squares principle. The second algorithm is developed with the aim to reduce the computational complexity, where the expectation-maximization principle is applied to estimate the channel and the impulsive noise iteratively. We compare the proposed algorithms by simulations and apply them to process the data collected during an experiment conducted in December 2015 in the estuary of the Swan River, Western Australia. The results show that both proposed algorithms have better performance than existing methods in mitigating impulsive noise in UA OFDM systems.**

***Index Terms*—EM, impulsive noise, OFDM, underwater acoustic communication.**

I. Introduction

The underwater acoustic (UA) channel is one of the most challenging channels for wireless communication due to the rapid dispersion in both time and frequency domains [1]. Orthogonal frequency-division multiplexing (OFDM) systems are proposed for UA communication recently due to their strong capability in mitigating inter-symbol interference with a large delay spread [2], [3].

However, UA OFDM systems are significantly impacted by impulsive noise introduced by natural sources and human activities [4], [5] which is one of key factors limiting the performance of UA communications [6], [7]. It is reported in [7] that impulsive noise can significantly degrade the performance of UA OFDM systems. One class of impulsive noise mitigation methods first detect the impulsive noise dominated samples through threshold testing and then adjust those samples by using blanking or clipping techniques in the time domain [6]. However, these methods fail to exploit the structure of OFDM signals, which leads to limited performance improvement. The second class of impulsive noise mitigation algorithms exploit the sparsity of impulsive noise [5], [8], and estimate the impulsive noise samples using the null subcarriers [9]. However, these methods require extra bandwidth for null subcarriers. The authors of [10] proposed to estimate the impulsive noise samples using both null and pilot subcarriers. However, the algorithm in [10] assumes static or semi-static channel impulse responses which are known to the receiver.

Manuscript received October 13, 2016; revised May 20, 2017; accepted August 17, 2017. Date of publication August 23, 2017; date of current version November 10, 2017. This work was supported by the Australian Research Council's Discovery Projects funding scheme (DP140102131). The review of this paper was coordinated by Dr. C. Cozzo. *(Corresponding author: Yue Rong.)*

P. Chen, Y. Rong, and S. Nordholm are with the Department Electrical and Computer Engineering, Curtin University, Bentley, WA 6845 Australia (e-mail: peng.ch@outlook.com; yue.rong@ieee.org; s.nordholm@curtin.edu.au).

Z. He is with the Key Laboratory of Universal Wireless Communication, Ministry of Education, Beijing University of Posts and Telecommunications, Beijing 100876, China, and also with the Key Laboratory of Underwater Acoustic Communication and Marine Information Technology, Ministry of Education, Xiamen University, Xiamen 361005, China (e-mail: hezq@bupt.edu.cn).

Color versions of one or more of the figures in this paper are available online at http://ieeexplore.ieee.org.

Digital Object Identifier 10.1109/TVT.2017.2743220

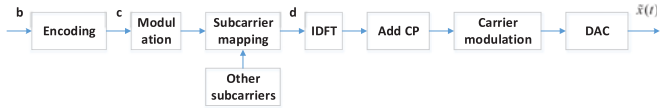

Fig. 1. Transmitter block diagram of a UA OFDM communication system.

In this paper, we propose two pilot-subcarrier based impulsive noise mitigation algorithms for UA OFDM communications. The first algorithm jointly estimates the channel impulse responses and the impulsive noise based on the least-squares (LS) principle. The second algorithm is developed with the aim to reduce the computational complexity, where the expectation-maximization (EM) method [11], [12] is applied to estimate the channel impulse responses and the impulsive noise iteratively. The estimated impulsive noise is then canceled from the received signal before channel equalization and channel decoding.

We evaluate the performance of the two proposed algorithms first by numerical simulations and then apply both algorithms to process the data collected during an experiment conducted in December 2015 in the estuary of the Swan River, Western Australia. The results show that compared with existing methods, both proposed algorithms yield an improved bit-error-rate (BER) and frame-error-rate (FER) performance.

II. System Model

In this paper, we consider a frame based coded UA OFDM communication system. As shown in Fig. 1, at the transmitter end, in each frame, a binary source data stream $\boldsymbol{b} = (b[1], \ldots, b[L_b])^T$ is encoded, interleaved, and punctured to form a coded sequence $\boldsymbol{c} = (c[1], \ldots, c[L_c])^T$ with length $L_c = R_m N_s N_b$, where $(\cdot)^T$ denotes the matrix (vector) transpose, L_b is the number of information-carrying bits in each frame, R_m denotes the modulation order, N_s is the number of data subcarriers, and N_b denotes the number of OFDM blocks in one frame. The coded sequence $\boldsymbol{c}$ is mapped into $N_s N_b$ data symbols taken from the phase-shift keying (PSK) or quadrature amplitude modulation (QAM) constellations. Then every N_s data symbols together with N_p quadrature PSK (QPSK) modulated pilot symbols are mapped into one OFDM symbol vector $\boldsymbol{d} = (d[1], \ldots, d[N_c])^T$, where N_p and $N_c \geq N_p + N_s$ are the number of pilot subcarriers and total subcarriers, respectively. We denote $\mathcal{I}_p$ as the indices of subcarriers with pilot symbols. We assume that pilot subcarriers are uniformly spaced and denote $\boldsymbol{d}_p$ as the pilot sequence in one OFDM block.

An OFDM symbol is converted to the time domain by the inverse discrete Fourier transform (DFT), resulting in the following baseband signal vector

$$\boldsymbol{x} = \boldsymbol{F}^H \boldsymbol{d} \tag{1}$$

where $(\cdot)^H$ denotes the Hermitian transpose and $\boldsymbol{F}$ is an $N_c \times N_c$ DFT matrix with the (i,k)-th entry of $1/\sqrt{N_c} e^{-j2\pi(i-1)(k-1)/N_c}$, $i, k = 1, \ldots, N_c$. The transmitter then prepends a cyclic prefix (CP) longer

0018-9545 © 2017 IEEE. Personal use is permitted, but republication/redistribution requires IEEE permission.
See http://www.ieee.org/publications_standards/publications/rights/index.html for more information.

than the channel delay spread to $\boldsymbol{x}$ and upshifts the signal. Let f_{sc} and T_{cp} denote the subcarrier spacing and the length of CP, respectively. Thus, the bandwidth of the transmitted signal is $B = f_{sc}N_c$ and the duration of one OFDM symbol is $T = 1/f_{sc}$, while the total length of one OFDM block is $T_{total} = T + T_{cp}$.

We consider that the frequency offset is properly removed at the receiver. Then after downshifting, low-pass filtering, and sampling the received signal at the rate of $1/B$ and removing the CP, we obtain the baseband discrete time samples of one OFDM symbol as

$$\boldsymbol{r} = \boldsymbol{F}^H \boldsymbol{D}\boldsymbol{h}_f + \boldsymbol{v} + \boldsymbol{w} = \boldsymbol{F}^H \boldsymbol{D}\boldsymbol{F}\boldsymbol{h}_t + \boldsymbol{v} + \boldsymbol{w} \tag{2}$$

where $\boldsymbol{D} = \mathrm{diag}(\boldsymbol{d})$ is a diagonal matrix taking $\boldsymbol{d}$ as the main diagonal elements, $\boldsymbol{r} = (r[1], \ldots, r[N_c])^T$ is the received signal vector, $\boldsymbol{v} = (v[1], \ldots, v[N_c])^T$ is the impulsive noise vector which is assumed to be sparse, $\boldsymbol{w} = (w[1], \ldots, w[N_c])^T$ is the complex Gaussian noise vector with zero-mean and variance σ^2. In (2), $\boldsymbol{h}_f = (h_f[1], \ldots, h_f[N_c])^T$ is a vector containing the channel frequency response at all N_c subcarriers and $\boldsymbol{h}_t = \boldsymbol{F}^H \boldsymbol{h}_f$ is the discrete time domain representation of the channel impulse response with a maximal delay of L_m.

From (2), the frequency domain representation of the received signal can be written as

$$\begin{aligned} \boldsymbol{r}_f &= \boldsymbol{F}\boldsymbol{r} \\ &= \boldsymbol{F}\boldsymbol{F}^H \boldsymbol{D}\boldsymbol{h}_f + \boldsymbol{F}\boldsymbol{v} + \boldsymbol{F}\boldsymbol{w} \\ &= \boldsymbol{D}\boldsymbol{h}_f + \boldsymbol{v}_f + \boldsymbol{w}_f \end{aligned} \tag{3}$$

where $\boldsymbol{v}_f = \boldsymbol{F}\boldsymbol{v}$ and $\boldsymbol{w}_f = \boldsymbol{F}\boldsymbol{w}$.

III. Proposed Approaches

Let us introduce an $N_p \times N_c$ matrix $\boldsymbol{P}$ having unit entry at the $(i, \mathcal{I}_p[i])$-th position, $i = 1, \ldots, N_p$, and zero elsewhere. From (3), the received signals at the pilot subcarriers can be written as

$$\boldsymbol{r}_p = \boldsymbol{P}\boldsymbol{D}\boldsymbol{h}_f + \boldsymbol{P}\boldsymbol{v}_f + \boldsymbol{P}\boldsymbol{w}_f = \boldsymbol{D}_p\boldsymbol{h}_p + \boldsymbol{v}_p + \boldsymbol{w}_p \tag{4}$$

where $\boldsymbol{D}_p = \mathrm{diag}(\boldsymbol{d}_p)$, $\boldsymbol{h}_p$ contains the channel frequency responses at N_p pilot subcarriers, $\boldsymbol{v}_p = \boldsymbol{P}\boldsymbol{v}_f$, and $\boldsymbol{w}_p = \boldsymbol{P}\boldsymbol{w}_f$.

We select $N_p \geq L_m$ since in this case $\boldsymbol{h}_f$ can be easily recovered from $\boldsymbol{h}_p$ without suffering from possible ambiguity, and we also assume that L_m is known to the receiver. Defining $\boldsymbol{P}_h$ as an $N_p \times L_m$ matrix with unit entry $\boldsymbol{P}_h[i, i]$ for $i = 1, \ldots, L_m$, and zero elsewhere, $\boldsymbol{h}_p$ can be written as

$$\boldsymbol{h}_p = \boldsymbol{F}_p\boldsymbol{P}_h\boldsymbol{h}_{p,t} \tag{5}$$

where $\boldsymbol{F}_p$ is an $N_p \times N_p$ DFT matrix[1] with the (i,k)-th entry of $1/\sqrt{N_p}e^{-j2\pi(i-1)(k-1)/N_p}$, $i, k = 1, \ldots, N_p$, and $\boldsymbol{h}_{p,t}$ is a vector with length L_m. Interestingly, with $N_c = KN_p$ and $\mathcal{I}_p[i] = (i-1)K + 1$, $i = 1, \ldots, N_p$, where K is an integer, there is $\boldsymbol{h}_t = [\sqrt{K}\boldsymbol{h}_{p,t}^T, \boldsymbol{0}_{1\times(N_c - L_m)}]^T$.

To obtain an estimation of $\boldsymbol{v}$ from $\boldsymbol{r}_p$, the positions of the impulsive noise need to be known to the receiver, in order to avoid ambiguity in estimation. This can be done by a threshold test, where the receiver firstly calculates the average power G of the current OFDM symbol and then collects the positions of possible impulsive noise into a vector $\mathcal{I}_I$ which satisfies

$$|r[\mathcal{I}_I[i]]|^2 > G\beta, \quad i = 1, \ldots, N_I. \tag{6}$$

Here N_I is the number of possible positions of impulsive noise and β is a threshold parameter discussed further in Section IV. Let us introduce

[1] As the pilot subcarriers are uniformly distributed among all subcarriers, the indices of the pilot subcarriers are not explicitly reflected in $\boldsymbol{F}_p$.

TABLE I
Procedure of the Proposed EM-Based Joint Channel and Impulsive Noise Estimation Algorithm

Initialization
$\boldsymbol{h}_{p,t}^{(0)} = (\boldsymbol{M}_h^H \boldsymbol{M}_h)^{-1}\boldsymbol{M}_h^H \boldsymbol{r}_p$
$\boldsymbol{v}_I^{(0)}[i] = \boldsymbol{r}[\mathcal{I}_I[i]],\ i = 1, ..., N_I$
For $s = 1, \ldots, S$
E-step: $\boldsymbol{y}_h^{(s)} = \boldsymbol{M}_h \boldsymbol{h}_{p,t}^{(s-1)} = \boldsymbol{D}_p\boldsymbol{F}_p\boldsymbol{P}_h\boldsymbol{h}_{p,t}^{(s-1)}$
$\boldsymbol{y}_v^{(s)} = \boldsymbol{M}_v \boldsymbol{v}_I^{(s-1)}$
$\boldsymbol{r}_h^{(s)} = \boldsymbol{y}_h^{(s)} + \beta_h\left(\boldsymbol{r}_p - \boldsymbol{y}_h^{(s)} - \boldsymbol{y}_v^{(s)}\right)$
$\boldsymbol{r}_v^{(s)} = \boldsymbol{y}_v^{(s)} + \beta_v\left(\boldsymbol{r}_p - \boldsymbol{y}_h^{(s)} - \boldsymbol{y}_v^{(s)}\right)$
M-step: $\boldsymbol{h}_{p,t}^{(s)} = \arg\min_{\boldsymbol{h}_{p,t}} \|\boldsymbol{r}_h^{(s)} - \boldsymbol{M}_h\boldsymbol{h}_{p,t}\|$
$\boldsymbol{v}_I^{(s)} = \arg\min_{\boldsymbol{v}_I} \|\boldsymbol{r}_v^{(s)} - \boldsymbol{M}_v\boldsymbol{v}_I\|$
end for

$\boldsymbol{v}_I$ as a vector containing all N_I samples of impulsive noise in one OFDM symbol. The impact of $\boldsymbol{v}_I$ on the N_p pilot subcarriers can be written as

$$\boldsymbol{v}_p = \boldsymbol{P}\boldsymbol{F}\boldsymbol{P}_I\boldsymbol{v}_I \tag{7}$$

where $\boldsymbol{P}_I$ is an $N_c \times N_I$ matrix indicating the position of the impulsive noise given by

$$\boldsymbol{P}_I[i,k] = \begin{cases} 1, & i = \mathcal{I}_I[k], k = 1, \ldots, N_I \\ 0, & \text{otherwise} \end{cases}.$$

Substituting (5) and (7) back into (4), we obtain

$$\begin{aligned} \boldsymbol{r}_p &= \boldsymbol{D}_p\boldsymbol{F}_p\boldsymbol{P}_h\boldsymbol{h}_{p,t} + \boldsymbol{P}\boldsymbol{F}\boldsymbol{P}_I\boldsymbol{v}_I + \boldsymbol{w}_p \\ &= \boldsymbol{M}_h\boldsymbol{h}_{p,t} + \boldsymbol{M}_v\boldsymbol{v}_I + \boldsymbol{w}_p \qquad (8) \\ &= \boldsymbol{M}_t\boldsymbol{\alpha} + \boldsymbol{w}_p \qquad (9) \end{aligned}$$

where

$$\begin{aligned} \boldsymbol{M}_h &= \boldsymbol{D}_p\boldsymbol{F}_p\boldsymbol{P}_h, \quad \boldsymbol{M}_v = \boldsymbol{P}\boldsymbol{F}\boldsymbol{P}_I \\ \boldsymbol{M}_t &= (\boldsymbol{M}_h,\ \boldsymbol{M}_v), \quad \boldsymbol{\alpha} = (\boldsymbol{h}_{p,t}^T,\ \boldsymbol{v}_I^T)^T. \end{aligned} \tag{10}$$

Based on (9), our first proposed algorithm named "LS-joint" is to estimate $\boldsymbol{\alpha}$ using the LS approach, which is given by

$$\hat{\boldsymbol{\alpha}} = (\boldsymbol{M}_t^H\boldsymbol{M}_t)^{-1}\boldsymbol{M}_t^H\boldsymbol{r}_p \tag{11}$$

where $(\cdot)^{-1}$ denotes matrix inversion. Then estimation of $\boldsymbol{h}_{p,t}$ and $\boldsymbol{v}_I$ can be obtained from $\hat{\boldsymbol{\alpha}}$ as (10). As inversion of $\boldsymbol{M}_t^H\boldsymbol{M}_t$ needs to be calculated in (11), the LS-joint algorithm has a computational complexity order of $\mathcal{O}((L_m + N_I)^3)$.

The second proposed algorithm named "EM-joint" is based on (8). Following the algorithm developed in [11] and [12], we define the "complete" data as

$$\boldsymbol{r}_h = \boldsymbol{M}_h\boldsymbol{h}_{p,t} + \boldsymbol{w}_h \tag{12}$$

$$\boldsymbol{r}_v = \boldsymbol{M}_v\boldsymbol{v}_I + \boldsymbol{w}_v \tag{13}$$

where $\boldsymbol{w}_h$ and $\boldsymbol{w}_v$ are zero-mean, independent and identically distributed Gaussian additive noise with variance σ_h^2 and σ_v^2, respectively, and $\sigma_h^2 + \sigma_v^2 = \sigma^2$. The procedure of the EM-based algorithm for the complete data in (12) and (13) is summarized in Table I, where the superscript (s) denotes the sth iteration, $\|\cdot\|$ stands for the vector Euclidean norm, and $\beta_h + \beta_v = 1$. After initialization, the EM-joint algorithm performs the E-step and the M-step iteratively until convergence.

As we assume that both $\boldsymbol{w}_h$ and $\boldsymbol{w}_v$ are zero-mean Gaussian vectors, the solutions to the two optimization problems in the M-step are given by

$$\boldsymbol{h}_{p,t}^{(s)} = (\boldsymbol{M}_h^H \boldsymbol{M}_h)^{-1} \boldsymbol{M}_h^H \boldsymbol{r}_h^{(s)} = \boldsymbol{P}_h^T \boldsymbol{F}_p^H \boldsymbol{D}_p^H \boldsymbol{r}_h^{(s)} \quad (14)$$

$$\boldsymbol{v}_I^{(s)} = (\boldsymbol{M}_v^H \boldsymbol{M}_v)^{-1} \boldsymbol{M}_v^H \boldsymbol{r}_v^{(s)} \quad (15)$$

where to obtain (14), we use the property that $\boldsymbol{M}_h^H \boldsymbol{M}_h = \boldsymbol{I}_{L_m}$ as the diagonal elements of $\boldsymbol{D}_p$ have unit radius due to the use of QPSK modulated pilot symbols. Here $\boldsymbol{I}_{L_m}$ denotes an $L_m \times L_m$ identity matrix. Based on the procedure in Table I and (14), (15), the computational complexity of the EM-joint algorithm is given by $\mathcal{O}(S(N_p \log_2 N_p + N_p N_I) + N_I^3)$ when N_p is power of 2. With $L_m = 64$, $N_I = 10$, $N_p = 128$, and $S = 10$, the complexity order of the LS-joint and the EM-joint algorithms are $\mathcal{O}(405224)$ and $\mathcal{O}(22760)$, respectively. Thus, the EM-joint algorithm has a lower computational complexity than the LS-joint approach.

Let $\hat{\boldsymbol{v}}_I$ and $\hat{\boldsymbol{h}}_{p,t}$ denote the estimation of $\boldsymbol{v}_I$ and $\boldsymbol{h}_{p,t}$, respectively, obtained either from the LS-joint algorithm or the EM-joint algorithm. Then $\boldsymbol{v}$ is estimated by $\hat{\boldsymbol{v}} = \boldsymbol{P}_I \hat{\boldsymbol{v}}_I$. Finally, $\hat{\boldsymbol{v}}$ is subtracted from the received signal $\boldsymbol{r}$ in (2) and the resulting signals are used for channel equalization and decoding using the estimated channel information $\hat{\boldsymbol{h}}_{p,t}$.

IV. Simulation Results

In this section, we study the performance of the proposed algorithms through numerical simulations. We simulate a UA OFDM system with 512 subcarriers including 325 data subcarriers, 128 uniformly spaced pilot subcarriers for channel estimation, and 59 null subcarriers. Each OFDM block contains a 100 sample long CP. Five OFDM blocks are transmitted in each channel realization and the simulation results are averaged through 10^4 channel realizations. The pilot symbols are modulated by QPSK constellations. The data symbols are modulated by 1/3 rate turbo encoded QPSK constellations. Considering the code puncturing, the number of information-carrying bits in each channel realization is $L_b = 1088$.

We simulate a UA channel with 15 paths. The arrival times of all paths follow a Poisson distribution with an average delay of 1 ms between two adjacent paths. The phase of each path follows a uniform distribution between $-\pi$ and π and remains constant for each channel realization. The amplitudes of the paths are Rayleigh distributed with variances following an exponentially decreasing profile. The ratio of the channel variances between the start and the end of the CP is 20 dB.

Let $\boldsymbol{u} = \boldsymbol{v} + \boldsymbol{w}$ represent the total additive noise in (2). A two-component Gaussian mixture (GM) model [9] is used to generate $\boldsymbol{u}$ with a probability density function of

$$f(u[i]) = (1-q)\mathcal{N}(0, \sigma^2) + q\mathcal{N}(0, \sigma_I^2),\ i = 1, \ldots, N_c \quad (16)$$

where $\mathcal{N}(\cdot)$ denotes the complex Gaussian distribution function, σ_I^2 is the variance of the impulsive noise, and q is the probability of occurrence of the impulsive noise. From (16), the total noise variance is $\sigma_{GM}^2 = (1-q)\sigma^2 + q\sigma_I^2$, and the signal-to-noise ratio (SNR) refers to the ratio of the transmitting signal power to the total noise variance σ_{GM}^2. In the simulations, similar to [9], we choose $q = 0.02$ and the ratio between σ_I^2 and σ^2 is set to 26 dB.

We first study the choice of the threshold β in (6). Fig. 2 shows the system coded BER versus the value of β when the blanking method is used to remove the samples $r[i]$ at positions determined by $\mathcal{I}_I$ in (6). It can be seen that the coded BER is not very sensitive to β. In fact, β can be selected between 4 and 8, within which the BER is acceptable.[2] In the following, we set $\beta = 5$ in the simulations and experiments.

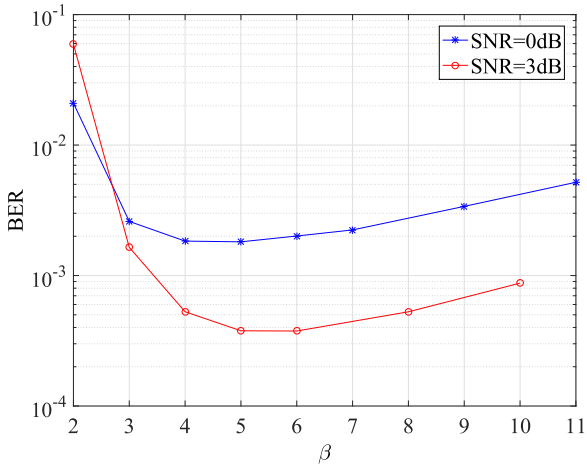

Fig. 2. BER of the blanking method versus β.

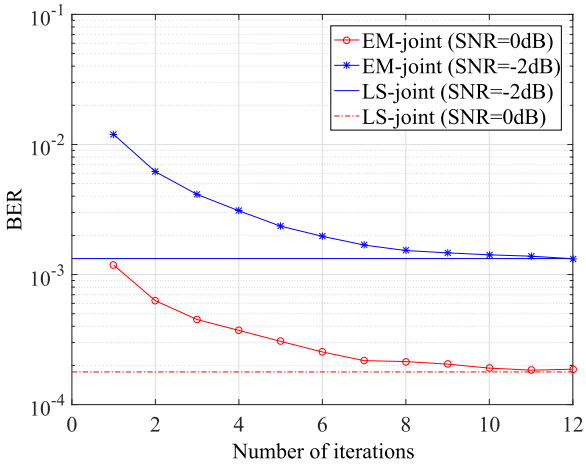

Fig. 3. BER of the EM-joint algorithm versus the number of iterations.

Fig. 3 shows the coded BER of the proposed EM-joint algorithm versus the number of iterations. We choose $\beta_h = \beta_v = 0.5$. The performance of the proposed LS-joint algorithm is also shown in Fig. 3 as a benchmark. It can be seen that the BER yielded by the proposed EM-joint algorithm converges to that of the LS-joint algorithm in 10 iterations in average.

Fig. 4 compares the coded BER of the two proposed algorithms, the blanking method, and the null subcarriers (NS)-based method. It can be observed that after 10 iterations, the BER of the EM-joint algorithm converges to that of the LS-joint algorithm throughout the whole SNR range. Moreover, the gap between the 10th and 4th iterations of the EM-joint algorithm is within 1 dB at low SNRs. When the SNR is larger than 0 dB, the performance of the EM-joint algorithm with 4 iterations tends to converge to that of the LS-joint algorithm. Both the blanking and the NS-based methods have higher BERs than the proposed algorithms. In particular, when the SNR is larger than -3 dB,

[2]For Gaussian channels, the optimal blanking threshold that maximizes the output SNR has been investigated in [13]. Note that UA channels are time-varying multipath fading channels with a large delay spread, which are much more complicated than the Gaussian channel [13] in determining the optimal threshold. To the best of our knowledge, for UA OFDM systems, a proper β is usually chosen based on the problem setup through simulations [9].

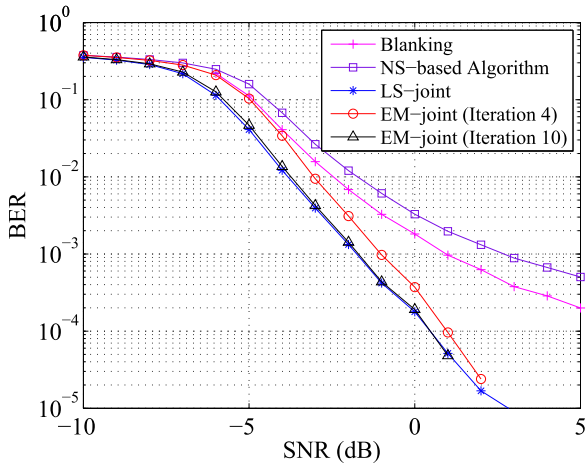

Fig. 4. BER comparison of various algorithms versus SNR.

Fig. 5. Transmitter and receiver locations during the experiment.

the gap between the blanking method, the NS-based method, and the proposed algorithms increases with the SNR.

V. Experiment Results and Discussions

In this section, we apply the proposed algorithms to process the data recorded during a UA communication experiment conducted in December 2015 in the estuary of the Swan River, Western Australia.

A. Experiment Arrangement and Channel Conditions

Key parameters of the experimental system are: carrier frequency $f_c = 12$ kHz, $B = 4$ kHz, $N_c = 512$, $T_{cp} = 25$ ms. Each frame contains five OFDM data blocks and one preamble block. The preamble block is used for synchronization and has the same length as a data block. Among the total 512 subcarriers, there are 325 data subcarriers, 128 uniformly spaced pilot subcarriers for channel estimation, 18 null subcarriers at each edge of the passband, and 23 subcarriers for frequency offset estimation. The pilot symbols are modulated by QPSK constellations. The data symbols are modulated by QPSK constellations encoded by either 1/2 or 1/3 rate turbo codes. Considering the code puncturing, the number of information-carrying bits in each frame is $L_b = 1632$ (1/2 rate) or $L_b = 1088$ (1/3 rate). Each transmission contains 500 frames with 250 frames for every modulation type.

The locations of the transmitter and receiver are shown in Fig. 5, where the distance between the transmitter and receiver was 936 meters. The water depth along the direct path varied between 2.5 and 6 meters, which was very shallow. Both the transmitter transducer and the receiver hydrophone were mounted 0.5 meter above the river bed on steel frames and were cabled to shore. The water depths at the transmitter and the receiver were 5 meters and 2.5 meters, respectively. The movement of the hydrophone and the transducer was small as they were attached to steel frames, resulting in ignorable Doppler drifting. As the hydrophone was located in warm shallow water close to a jetty, there was significant amount of highly impulsive snapping shrimp noise. Another source of impulsive noise during the experiment was from waves breaking at the jetty piers whose intensity increases with the wind speed. To investigate the impact of wind on the breaking wave noise, the same data file was transmitted three times during the day under different wind conditions. The data files recorded at the receiver during three transmissions were named T83, T84, and T85, respectively.

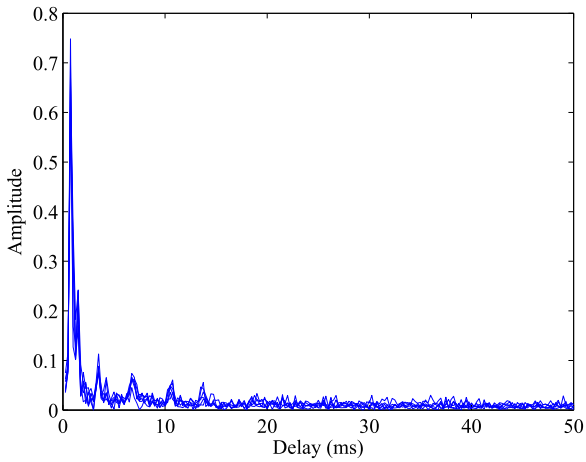

Fig. 6. Amplitude of channel impulse response estimated by the preamble blocks in the T83 file.

To study the channel conditions, we perform channel estimation using the preamble blocks based on the LS estimator. Fig. 6 illustrates the amplitude of the estimated channel impulse responses of several data frames in the T83 file where the preamble blocks are only slightly interfered by the impulsive noise. It can be seen that in this case, the channel estimation result is reasonable. In particular, we can observe from Fig. 6 that the maximal channel delay spread in the experiment is about 15 ms which is shorter than T_{cp}. Moreover, it can be seen that there are seven notable paths between the transmitter and the receiver.

B. Receiver Performance

Since the maximum delay of the UA channel is around 15 ms during the experiment as shown in Fig. 6, we set $L_m = 64$ and choose $\beta_h = \beta_v = 0.5$ for the proposed EM-joint algorithm. The BER (both raw and coded) and the FER performances of the following channel estimation and impulsive noise mitigation algorithms are compared in Tables II IV for three recorded files.

1) LS channel estimator without the blanking operation.
2) LS channel estimator after blanking of the impulsive samples detected at the positions of $\mathcal{I}_I$ (6).

TABLE II
PERFORMANCE COMPARISON FOR THE T83 FILE

Modulation Type	Method	Raw BER	Coded BER	FER
QPSK, 1/3 rate	LS w/o blanking	6.2%	0.2%	0.4%
	LS + blanking	5.2%	0	0
	LS-joint	3.2%	0	0
	EM-joint	3.2%	0	0
QPSK, 1/2 rate	LS w/o blanking	5.6%	0.3%	1.6%
	LS + blanking	4.7%	0	0
	LS-joint	3.0%	0	0
	EM-joint	2.9%	0	0

TABLE III
PERFORMANCE COMPARISON FOR THE T84 FILE

Modulation Type	Method	Raw BER	Coded BER	FER
QPSK, 1/3 rate	LS w/o blanking	18.7%	10.9%	50.4%
	LS + blanking	15.5%	1.3%	7.3%
	LS-joint	12.8%	0.2%	0.8%
	EM-joint	12.5%	0.2%	0.8%
QPSK, 1/2 rate	LS w/o blanking	18.1%	22.5%	93.6%
	LS + blanking	14.6%	15.9%	84.7%
	LS-joint	12.0%	4.3%	30.2%
	EM-joint	11.7%	3.8%	25.8%

TABLE IV
PERFORMANCE COMPARISON FOR THE T85 FILE

Modulation Type	Method	Raw BER	Coded BER	FER
QPSK, 1/3 rate	LS w/o blanking	13.5%	1.6%	6.4%
	LS + blanking	11.2%	0	0
	LS-joint	8.6%	0	0
	EM-joint	8.5%	0	0
QPSK, 1/2 rate	LS w/o blanking	15.0%	15.3%	71.6%
	LS + blanking	11.7%	3.9%	24.8%
	LS-joint	9.4%	0.3%	2.4%
	EM-joint	9.3%	0.2%	1.6%

3) Proposed LS-joint algorithm.
4) Proposed EM-joint algorithm with 10 iterations.

It can be seen from Table II that the two proposed algorithms achieve a lower raw BER than the blanking method. Interestingly, since the T83 file is only slightly affected by impulsive noise, both the blanking method and the two proposed algorithms are able to obtain zero coded BER and FER over the investigated data.

As the T84 file is severely contaminated by impulsive noise, it can be seen from Table III that although the proposed algorithms successfully reduce the raw and coded BER for 1/2 rate signals, the system FER remains high, indicating that the channel condition of the T84 file is very challenging for high rate signals. For the 1/3 rate signals, the proposed EM-joint algorithm brings 3.0%, 1.1%, and 6.5% decrease in the raw BER, coded BER, and FER, respectively, compared with the blanking method.

As the T85 file suffers from middle level impulsive noise, similar to the T83 file, it can be seen from Table IV that for the 1/3 rate signals the blanking method and the two proposed algorithms are able to obtain zero coded BER and FER over the investigated data. However, for 1/2 rate signals, both proposed algorithms clearly outperform the blanking method. Compared with the blanking method, the proposed EM-joint algorithm introduces 2.4%, 3.7%, and 23.2% decrease in the raw BER, coded BER, and FER, respectively. We also observe from Tables III and IV that both proposed algorithms have a similar BER and FER performance. Considering that the EM-joint algorithm has a lower computational complexity, it is more interesting for practical UA OFDM systems.

VI. CONCLUSION

We have proposed an LS-based and an EM-based joint channel estimation and impulsive noise mitigation algorithms for UA OFDM systems. The proposed algorithms utilize the pilot subcarriers to estimate the impulsive noise and channel impulse response. Compared with the existing blanking method, the proposed algorithms successfully improve the accuracy of channel estimation and the performance of impulsive noise mitigation by utilizing the structure of OFDM signals. We applied the proposed algorithms to process the data collected during a recent UA communication experiment. The results show that when the received signals are only slightly influenced by impulsive noise, both the proposed algorithms and the blanking method have similar performance. When the received signals are severely impacted by impulsive noise, the proposed algorithms outperform the blanking method.

REFERENCES

[1] M. Stojanovic and J. Preisig, "Underwater acoustic communication channels: Propagation models and statistical characterization," *IEEE Commun. Mag.*, vol. 47, no. 1, pp. 84–89, Jan. 2009.
[2] Z. Wang, S. Zhou, J. Catipovic, and P. Willett, "Asynchronous multiuser reception for OFDM in underwater acoustic communications," *IEEE Trans. Wireless Commun.*, vol. 12, no. 3, pp. 1050–1061, Mar. 2013.
[3] H. Yan *et al.*, "DSP based receiver implementation for OFDM acoustic modems," *Elsevier J. Phys. Commun.*, vol. 5, no. 1, pp. 22–32, Mar. 2012.
[4] J. Hildebrand, "Anthropogenic and natural sources of ambient noise in the ocean," *Marine Ecol. Progress Series*, vol. 395, pp. 5–20, Dec. 2009.
[5] M. Chitre, S. Kuselan, and V. Pallayil, "Ambient noise imaging in warm shallow waters; robust statistical algorithms and range estimation," *J. Acoust. Soc. Amer.*, vol. 132, no. 2, pp. 838–847, Aug. 2012.
[6] T. Suzuki, H. M. Tran, and T. Wada, "An underwater acoustic OFDM communication system with shrimp (impulsive) noise cancelling," in *Proc. Int. Conf. Comput. Manag. Telecommun.*, Da Nang, Vietnam, Apr. 2014, pp. 152–156.
[7] M. Chitre, S. H. Ong, and J. Potter, "Performance of coded OFDM in very shallow water channels and snapping shrimp noise," in *Proc. MTS/IEEE OCEANS*, Washington, DC, USA, Sep. 2005, vol. 2, pp. 996–1001.
[8] M. A. Chitre, J. R. Potter, and S. H. Ong, "Optimal and near-optimal signal detection in snapping shrimp dominated ambient noise," *IEEE J. Ocean. Eng.*, vol. 31, no. 2, pp. 497–503, Apr. 2006.
[9] X. Kuai, H. Sun, S. Zhou, and E. Chen, "Impulsive noise mitigation in underwater acoustic OFDM systems," *IEEE Trans. Veh. Technol.*, vol. 65, no. 10, pp. 8190–8202, Oct. 2016.
[10] J. Lin, M. Nassar, and B. L. Evans, "Impulsive noise mitigation in powerline communications using sparse bayesian learning," *IEEE J. Select. Areas Commun.*, vol. 31, no. 7, pp. 1172–1183, Jul. 2013.
[11] M. Feder and E. Weinstein, "Parameter estimation of superimposed signals using the EM algorithm," *IEEE Trans. Acoust. Speech Signal Process.*, vol. 36, no. 4, pp. 477–489, Apr. 1988.
[12] Y. Xie and C. N. Georghiades, "Two EM-type channel estimation algorithms for OFDM with transmitter diversity," *IEEE Trans. Commun.*, vol. 51, no. 1, pp. 106–115, Jan. 2003.
[13] S. Zhidkov, "Performance analysis and optimization of OFDM receiver with blanking nonlinearity in impulsive noise environment," *IEEE Trans. Veh. Technol.*, vol. 55, no. 1, pp. 234–242, Jan. 2006.